

UNCLASSIFIED

AD NUMBER
ADB225305
NEW LIMITATION CHANGE
TO Approved for public release, distribution unlimited
FROM Distribution authorized to U.S. Gov't. agencies only; Proprietary Info.; Sep 96. Other requests shall be referred to Commander, U.S Army Medical Research and Materiel Command, Attn: MCMR-RMI-S, Fort Detrick, Frederick, MD 21702-5012.
AUTHORITY
DA, US Army Med Research and Mat Cmd, ltr dtd 22 Jun 2000, MCMR-RMI-S [70-1y], Dep Ch of Staff Info Mgt, Ft Detrick, MD

THIS PAGE IS UNCLASSIFIED

AD _____

GRANT NUMBER DAMD17-94-J-4367

TITLE: Development of an Inverse Technique to Estimate the
Ultrasound Field During Chest Wall and Breast Hyperthermia

PRINCIPAL INVESTIGATOR: Charles L. Thomas, Ph.D.

CONTRACTING ORGANIZATION: University of Utah
Salt Lake City, UT 84112

REPORT DATE: August 1996

TYPE OF REPORT: Annual

PREPARED FOR: Commander
U.S. Army Medical Research and Materiel Command
Fort Detrick, Frederick, Maryland 21702-5012

DISTRIBUTION STATEMENT: Distribution authorized to U.S.
Government agencies only (proprietary information, Sep 96).
Other requests for this document shall be referred to Commander,
U.S. Army Medical Research and Materiel Command, ATTN:
MCMR-RMI-S, Fort Detrick, Frederick, MD 21702-5012.

The views, opinions and/or findings contained in this report are
those of the author(s) and should not be construed as an official
Department of the Army position, policy or decision unless so
designated by other documentation.

19970618 139

THIS QUALITY DISTRIBUTION 1

REPORT DOCUMENTATION PAGE

Form Approved
OMB No. 0704-0188

Public reporting burden for this collection of information is estimated to average 1 hour per response, including the time for reviewing instructions, searching existing data sources, gathering and maintaining the data needed, and completing and reviewing the collection of information. Send comments regarding this burden estimate or any other aspect of this collection of information, including suggestions for reducing this burden, to Washington Headquarters Services, Directorate for Information Operations and Reports, 1215 Jefferson Davis Highway, Suite 1204, Arlington, VA 22202-4302, and to the Office of Management and Budget, Paperwork Reduction Project (0704-0188), Washington, DC 20503.

1. AGENCY USE ONLY (Leave blank)		2. REPORT DATE August 1996	3. REPORT TYPE AND DATES COVERED Annual (1 Aug 95 - 31 Jul 96)
4. TITLE AND SUBTITLE Development of an Inverse Technique to Estimate the Ultrasound Field During Chest Wall and Breast Hyperthermia			5. FUNDING NUMBERS DAMD17-94-J-4367
6. AUTHOR(S) Charles L. Thomas, Ph.D.			
7. PERFORMING ORGANIZATION NAME(S) AND ADDRESS(ES) University of Utah Salt Lake City, UT 84112			8. PERFORMING ORGANIZATION REPORT NUMBER
9. SPONSORING/MONITORING AGENCY NAME(S) AND ADDRESS(ES) U.S. Army Medical Research and Materiel Command Fort Detrick Frederick, Maryland 21702-5012			10. SPONSORING/MONITORING AGENCY REPORT NUMBER
11. SUPPLEMENTARY NOTES			
12a. DISTRIBUTION / AVAILABILITY STATEMENT Distribution authorized to U.S. Government agencies only; proprietary information, Sep 96. Other requests for this document shall be referred to Commander, U.S. Army Medical Research and Materiel Command, ATTN: MCMR-RMI-S, Fort Detrick, Frederick, MD 21702-5012			12b. DISTRIBUTION CODE
13. ABSTRACT (Maximum 200) It is the goal of this research to provide improved numerical modeling of ultrasound propagation through breast tissue and the post-mastectomy chest wall for use in patient treatment planning of hyperthermia cancer treatments. With this improved model the clinician can plan an ultrasound hyperthermia treatment so as to produce the required thermal dose while minimizing patient pain due to excessive temperature or ultrasound-tissue interactions. A clinical system is being constructed to combine model results with experiments in an inverse technique to estimate the absorbed power field in the breast and chest wall during ultrasound hyperthermia. This improved planning will aid the clinicians in providing better hyperthermia treatments which will improve treatment response rates.			
14. SUBJECT TERMS Breast Cancer			15. NUMBER OF PAGES 30
			16. PRICE CODE
17. SECURITY CLASSIFICATION OF REPORT Unclassified	18. SECURITY CLASSIFICATION OF THIS PAGE Unclassified	19. SECURITY CLASSIFICATION OF ABSTRACT Unclassified	20. LIMITATION OF ABSTRACT limited

FOREWORD

Opinions, interpretations, conclusions and recommendations are those of the author and are not necessarily endorsed by the US Army.

Where copyrighted material is quoted, permission has been obtained to use such material.

Where material from documents designated for limited distribution is quoted, permission has been obtained to use the material.

Citations of commercial organizations and trade names in this report do not constitute an official Department of Army endorsement or approval of the products or services of these organizations.


In conducting research using animals, the investigator(s) adhered to the "Guide for the Care and Use of Laboratory Animals," prepared by the Committee on Care and Use of Laboratory Animals of the Institute of Laboratory Resources, National Research Council (NIH Publication No. 86-23, Revised 1985).

For the protection of human subjects, the investigator(s) adhered to policies of applicable Federal Law 45 CFR 46.

In conducting research utilizing recombinant DNA technology, the investigator(s) adhered to current guidelines promulgated by the National Institutes of Health.

In the conduct of research utilizing recombinant DNA, the investigator(s) adhered to the NIH Guidelines for Research Involving Recombinant DNA Molecules.

In the conduct of research involving hazardous organisms, the investigator(s) adhered to the CDC-NIH Guide for Biosafety in Microbiological and Biomedical Laboratories.


PI - Signature 9-9-96
Date

CLT 2-6-97

Contents

Introduction	3
Revised Task Description and Milestones	5
Outline of Accomplishments	5
First Year Summary	6
Second Year Accomplishments	7
Future Work	16
References	16
Appendix A: Log Spectral Difference	19
Appendix B: Ultrasound Propagation Models	22

Introduction

Hyperthermia has been shown to be an efficacious adjuvant therapy in the treatment of recurrent breast cancer.[1,2,3] One of the most flexible and proven methods to induce hyperthermia is ultrasound. In order to optimally utilize such clinical devices it is essential that the operator have the ability to accurately plan a treatment. The clinical hyperthermia situation is diagrammed in Figure 1. A treatment plan consists of a defined motion path and applied transducer power that will raise the temperature of the tumor to a desired set point for a specified time, while minimizing the effect on surrounding tissue. The treatment plan must be adjusted for tissue geometry, absorption, and desired temperature history specific to each patient. Planning a treatment begins with the accurate estimation of the absorbed power field created by the ultrasound transducer. Thus, the ability to accurately estimate this field is critical to producing a proper and effective treatment plan.

Goals

It is the goal of this research to provide improved numerical modeling of ultrasound propagation through breast tissue and the post-mastectomy chest wall for use in patient treatment planning of hyperthermia cancer treatments. With this improved model the clinician can plan an ultrasound hyperthermia treatment so as to produce the required thermal dose while minimizing patient pain due to excessive temperature or ultrasound-tissue interactions. A clinical system is being constructed to combine model results with experiments in an inverse technique to estimate the absorbed power field in the breast and chest wall during ultrasound hyperthermia. This improved planning will aid the clinicians in providing better hyperthermia treatments which will improve treatment response rates.

The system under development consists of the following subsystems:

1. An ultrasonic B-mode imager based clinical data acquisition system to obtain patient anatomy, measure attenuation, and measure absorbed power.
2. A clinical technique using the ultrasound treatment system to directly measure absorbed power at specific points.
3. An improved model of ultrasound propagation through breast tissue.
4. An inverse technique that integrates experimental measurements and modeling results to obtain the "best" prediction of the ultrasound power deposition field.

The B-mode diagnostic ultrasound imager in Subsystem 1 is used to construct a geometric model based upon each patient's anatomy and to measure the ultrasound attenuation coefficient at selected areas within the tissue region. In Subsystem 2 the clinical treatment system is used in a scanning protocol to locate thermocouples imbedded in the breast tissue. The response of these thermocouples to the scanned ultrasound gives a direct measure of the power deposition at that point. Subsystem 3 is an ultrasound propagation and power deposition model. For this model we are currently considering 2 options: a) Hybrid Model - Ultrasound propagation from the transducer into the breast is modeled with a hybrid of Green's function solutions used in the homogenous water region and a finite element solution of the acoustic wave equation in the inhomogeneous breast region. b) Parabolic Model - This is a forward marching parabolic model that is quite fast, but does not take into account reflected energy at interfaces. Subsystem 4 is an iterative inverse technique that optimizes the parameters of the power deposition model by forcing the model

results to match the experimental measurements. The model is used to predict the power deposition at the thermocouple locations, the error between model and experiment is measured, and the error values are used to adjust the model parameters for the next iteration.

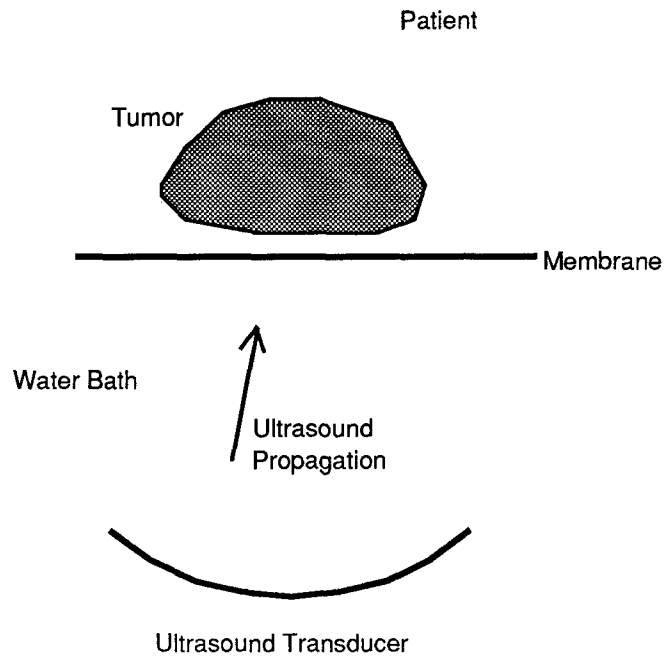


Figure 1: Diagram of the clinical situation for a hyperthermia treatment of the breast or chest wall area.

Revised Task Description and Milestones:

As in any research project, during the course of the project the researchers often discover that some tasks are easier than expected; other tasks are difficult or impossible and are replaced with alternative solutions. As can be seen from the project description in the introduction, this has certainly occurred here. Difficulties with the initial modeling techniques have resulted in a search for alternatives. Investigation of the Geometry Acquisition/Registration problem has resulted in expanded goals in this area. In an attempt to clarify what has been accomplished and what is left to accomplish in this research program, the original Task Description and Milestones chart has been modified to reflect the current project tasks and goals.

Task Description and Milestones:	Quarter															
	1	2	3	4	5	6	7	8	9	10	11	12	13	14	15	16
Finite Element Model	x	x	x	x	x	x	x	x								
Hybrid Green's Function Model					x	x	x	x	o	o						
Parabolic Model					x	x	x	x	o	o	o	o				
Inverse Technique	x	x							o	o	o	o	o	o	o	o
Ultrasonic Hardware Development	x	x	x	x												
Attenuation Measurement 1D			x	x	x	x	x	x								
Attenuation Measurement 3D									o	o	o	o	o	o	o	
Geometry Acquisition/Registration									o	o	o	o	o	o	o	o
<i>in vivo</i> SAR technique	x								o	o	o	o	o	o	o	o
System Integration/Phantom Tests										o	o	o	o	o		
Clinical Data Gathering												o	o	o	o	o

Outline of Accomplishments:

1st Year Accomplishments:

Subsystem 1: Geometry Acquisition and Attenuation Measurement

- Acquisition of ultrasonic B-scan instrument.
- Development of interface hardware to isolate analog A-scan information.
- Acquisition of high speed A/D system and development of control software.
- Investigation of reflection based acoustic attenuation measurement techniques.

Subsystem 2: Experimental SAR Measurement

- Initial discussions and verification of equipment.

Subsystem 3: Model Development

- Development and testing of a 2D finite element based model.
- Identification of alternative solutions.

Subsystem 4: Inverse Technique

- Initial discussions.

2nd Year Accomplishments:

Subsystem 1: Geometry Acquisition and Attenuation Measurement

- Development of Log Spectral Difference software for measuring the acoustic attenuation from a single A-line.
- Development and testing of a Force/Balance test apparatus for direct measurement of acoustic attenuation.

Subsystem 2: Experimental SAR Measurement

- No work accomplished.

Subsystem 3: Model Development

- Extension of the 2D FE model to three dimensions. Combination of the FE model with an integral method model to improve the speed of the model.
- Development of a 3D parabolic model as a much faster, possibly less accurate alternative.
- Development of a 3D Green's Function model for use as the "gold standard" with which the other models will be compared.
- Initial model comparisons.

Subsystem 4: Inverse Technique

- No progress.

First Year Summary

The first year efforts centered on initial development of the ultrasound propagation models and acquisition and initial development of the diagnostic ultrasound equipment. A brief discussion of these efforts is included below. For more detailed information refer to the first year progress report.

Initial modeling efforts focused on two potential methods: Green's Function Method where the transducer face is modeled as a distribution of point sources, and the Finite Element Method where FE techniques are used to solve the acoustic wave equation. A two dimensional FE code was written, and verification runs were under way at the end of the first year. The results of these runs and further investigation of the modeling possibilities led to the development of a hybrid model that combines the features of the two techniques to provide improved speed and accuracy. Details of this model are discussed in the second year accomplishments below.

During the first year a diagnostic ultrasound B-mode imager was acquired. This imager was modified to allow access to the raw RF waveform (A-line) for each scan line of the B-mode image. A schematic of the resulting system is shown in Figure 2. The ultrasound unit (Scanner 250, Pie Medical USA 3535 Route 66, Neptune NJ 07753) was modified to output the RF signals along with sync signals. A custom hardware selection device was constructed to read these signals and output a single A-line. A PC based data acquisition system was acquired that allows digitization of the A-line signals. Once the data is in the PC it is available for use in software techniques to estimate the ultrasonic

attenuation field in the tissue. Along with the hardware development, software was developed to operate the hardware and perform the attenuation estimate.[4]

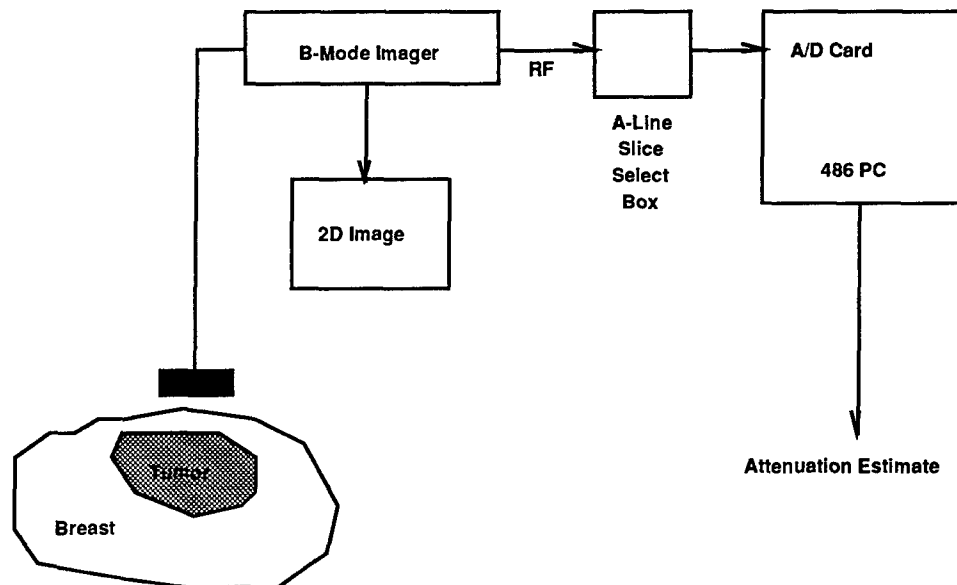


Figure 2: Diagram of the B-mode ultrasound imager based clinical data acquisition system used to obtain patient geometry and measure attenuation.

Second Year Accomplishments

The second year accomplishments will be discussed in terms of the four subsystems identified above.

Subsystem 1: Ultrasound Based Anatomy and Attenuation Measurement

The B-mode imager will provide two important functions: a) acquisition of 2D B-mode images for construction of a 3D geometric model of patient anatomy and b) provide an estimate of the ultrasound absorption field in the body tissue to provide starting point parameters for the models.

Geometric Model Construction

Figure 2 diagrams the ultrasound based data acquisition system which consists of a B-mode ultrasound imager to acquire patient geometry. This image will serve as the diagnostic medical image that the geometric model will be based upon.

The construction of the geometric model is the most labor intensive step in solving for the propagation of ultrasound through tissue. In this step, it is necessary to determine the exterior boundary, the boundary conditions, and the internal spatial distribution of material properties and enter these data into the computer for analysis. The most common technique in use today is to base the geometric model upon a standard diagnostic medical image such as CT or MRI.[5] Regions of interest are then traced out over this image and the interior region is meshed for the appropriate numerical solution.

In the first stage of this work only two-dimensional models will be constructed based upon a single image from the B-mode scanner (see Figure 3). The imager is equipped with a software measurement package and a hard copy output device. The operator will capture the image of interest, determine regions of constant material properties, measure the dimensions of these regions, and print-out that image. Once the geometric information is obtained, a two dimensional unstructured mesh generator[6] is used to mesh the domain with quadrilateral elements for a finite element analysis. (Note: this is all that was planned in the original proposal.)

The next step is to acquire a series of spatially distributed images and assemble them into a 3D model. The clinical solution will require the physician or assistant to sketch the important anatomical features (skin, tumor, bone) on a series of 2D "slices". The clinical software will combine the 2D geometry into a 3D representation appropriate for input to the model.

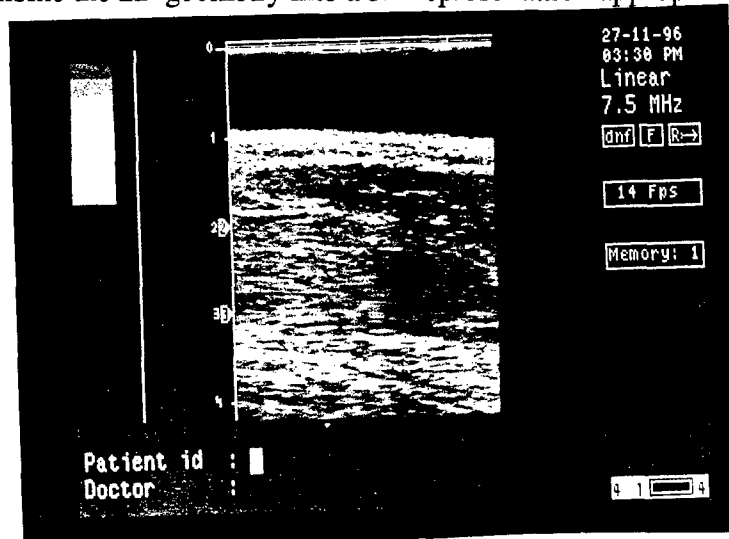


Figure 3: This is a typical image produced by the B-mode ultrasound scanner.

Ultrasonic Attenuation Measurement

The power deposited at a specific point in tissue by the ultrasound transducer depends on the intensity of the sound field at that point and the absorption coefficient of the tissue at that point. Clearly, the intensity at a point depends on the initial intensity and the attenuation of the signal in the tissue. This attenuation is due to scattering, absorption, and geometric attenuation. Previous research has shown that the attenuation is highly variable within human body tissue, with measurements varying significantly for different tissue types, for similar tissue on different subjects, and even for the same tissue on the same patient on different days.[7,8,9,10] Thus, it is important to measure the attenuation of the ultrasonic signal *in vivo* on the patient at the treatment site.

Using the data acquisition system shown in Fig. 2, it is possible to estimate the attenuation of the ultrasound at different points in the patient tissue from the RF signal collected. This is accomplished using a Log Spectral Difference technique.[8,9,11] Details of this technique are discussed in Appendix A. It is important to note that Log Spectral Difference is one of several possible techniques and provides an *estimate* of the attenuation.[6] For this reason it is important to test the accuracy of the technique with other measurements.

Tests were conducted where the acoustic attenuation of a series of samples were measured using both log spectral difference and the Force Balance technique. Using the Force Balance technique the force generated when an acoustic wave impinges on an absorbing material is measured and related to the power of the wave. Using this technique it is possible to make a direct measurement of the attenuation or absorbed power. For this reason, the force balance technique is used as a standard to which the log spectral difference measurements are compared. While it is generally considered accurate and reliable, the force balance technique is not suitable for use in the clinical experiments due to geometric constraints.

Using the techniques described above, initial tests have been run on chicken breast to compare the results of the two techniques discussed above. Using the Log Spectral Difference Technique, the normalized attenuation coefficient for the chicken was measured as $0.1608 \text{ Nepers} \times \text{cm}^{-1} \times \text{MHz}^{-1}$. [4] Using the Force Balance system measured values ranged from 0.108 to $0.138 \text{ Nepers} \times \text{cm}^{-1} \times \text{MHz}^{-1}$. These values are of the same magnitude as values reported in the literature ($0.06 - 0.13 \text{ Nepers} \times \text{cm}^{-1} \times \text{MHz}^{-1}$). [12]

Subsystem 2: Absorbed Power Measurement

While the log spectral difference technique is convenient because it is non-invasive and allows measurement of the attenuation field within the tissue, it does not give exact measurements. Attenuation field data received from the B-scan system will be used as a starting point for the parameters used in the math models. If the inverse optimization scheme is to be successful, it is also necessary to make precise experimental measurements of the power deposited in the tissue by the treatment transducer.

This research is based upon an existing clinical system which provides all the tools necessary to perform power deposition measurements using a thermal technique. Details of the original technique can be found in [13,14] with more recent applications discussed in [15,16,17,18]. The relation between the absorbed power due to relaxation (as measured by the thermal techniques) and the acoustic pressure calculated by the numerical models was put forth by Nyborg. [19]

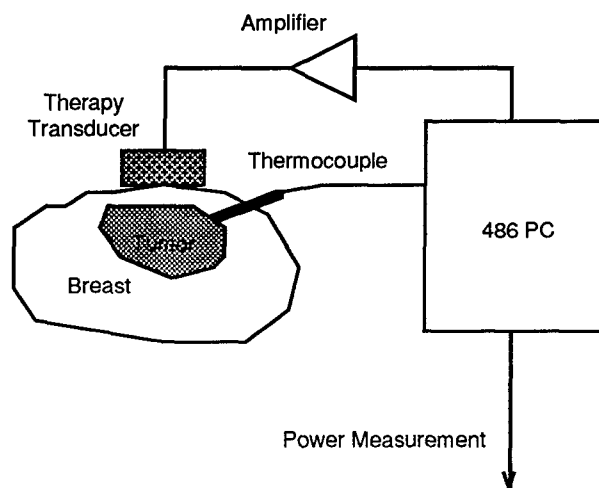


Figure 4: This is a schematic diagram of the operation of the absorbed power measurement test.

Conceptually these tests will use the schematic shown in Fig. 4. The treatment transducer will be scanned at low power to identify the locations of the imbedded thermocouples. When the focus of the transducer is brought into the vicinity of a thermocouple, the thermocouple will exhibit a sharp temperature rise. Once the thermocouple is located, the transducer focus will be centered on that location, and power applied. For a given input power, the rate of increase in temperature measured by the thermocouple is a direct measure of the absorbed power at that point (and also related to the attenuation in the tissue between the transducer and the measurement point). The temperature changes experienced during these tests should be brief, with maximum temperatures significantly below treatment levels.

Subsystem 3: Ultrasound Propagation Modeling

Results of the two models currently under investigation are discussed here. Details of their development are included in Appendix B.

A hybrid numerical model using integral methods to solve for the acoustic displacements in the region where the ultrasound propagates from the transducer to the patient's skin and using a finite element solution of the wave equation for propagation in the body has been developed and preliminary tests have been performed. Since the model predicts the displacements and stresses propagating through the tissue, it automatically accounts for reflections and transmission at interfaces. As a result we see in preliminary results a tendency for standing waves to be formed caused by the artificial boundary conditions set at the edges of the model space (see Appendix B for details). The model currently has difficulty handling the frequencies produced by the treatment transducers. This results from the fact that the finite element mesh must use smaller elements at higher frequencies. This results in more elements for the same physical model size and an exponential increase in computation time.

A second model, based on the parabolic equation method has also been developed and has undergone preliminary tests. The parabolic equation method is a very efficient method for modeling acoustic wave propagation through low contrast acoustic materials. This solution technique is somewhat more of an approximation than the hybrid model, but because of the source/receiver geometry used in the hyperthermia experiment, and the relatively low contrast of breast tissue, it is possible to utilize this efficient approximation. The resulting speed-up relative to the finite element method is dependent upon the contrast but is found to be fairly large. This is especially true of the large 3D problems simulated in this report.

Speed Issues:

We have found that there is difficulty in using standard mesh-generating code to model a 7.5 by 7.5 by 7.5 cm piece of tissue at 500 KHz. However, we have carried out simulations at the full 2 MHz using the Parabolic Fourier Marching method. The operating frequency of the device is 2 MHz so we are confident that the present code will serve as a suitable model, provided, of course that the accuracy can be verified.

This difference in speed is due in part to variations in the density of spatial sampled required for the various models. The parabolic marching method requires spatial sampling at only $\lambda/2$, where λ is the wavelength in the slowest material present, at the highest frequency. This yields a savings of a factor of $2^3 = 8$ over the integral equation method

which requires a sampling of $\lambda/4$. The finite element solution requires a sampling of approximately $\lambda/8$, so the parabolic method gives an improvement of roughly $4^3 = 64$.

Figures 5 and 6 demonstrate the kind of information available from the models. They have been duplicated here from Appendix B for convenience. In Figure 5 we see a continuous plane wave propagating from the left, entering the body through a vertical skin layer. The wave travels through an elliptical fatty region and into the spherical tumor. The left hand figure shows the wave energy density that tends to get weaker as the wave moves to the right. Note that the tumor absorbs most of the wave energy resulting in a "dark" shadow behind the tumor. The right hand figure shows the energy absorbed. Note that in the water and normal tissue the absorbed energy is low; even when the wave energy is high. Then there is an increase in absorbed energy as the wave passes into the tumor. This results from the higher absorption coefficient in the tumor. This effect is shown more clearly in Fig. 6 which is a line plot of the absorbed energy along a central axis in Fig. 5.

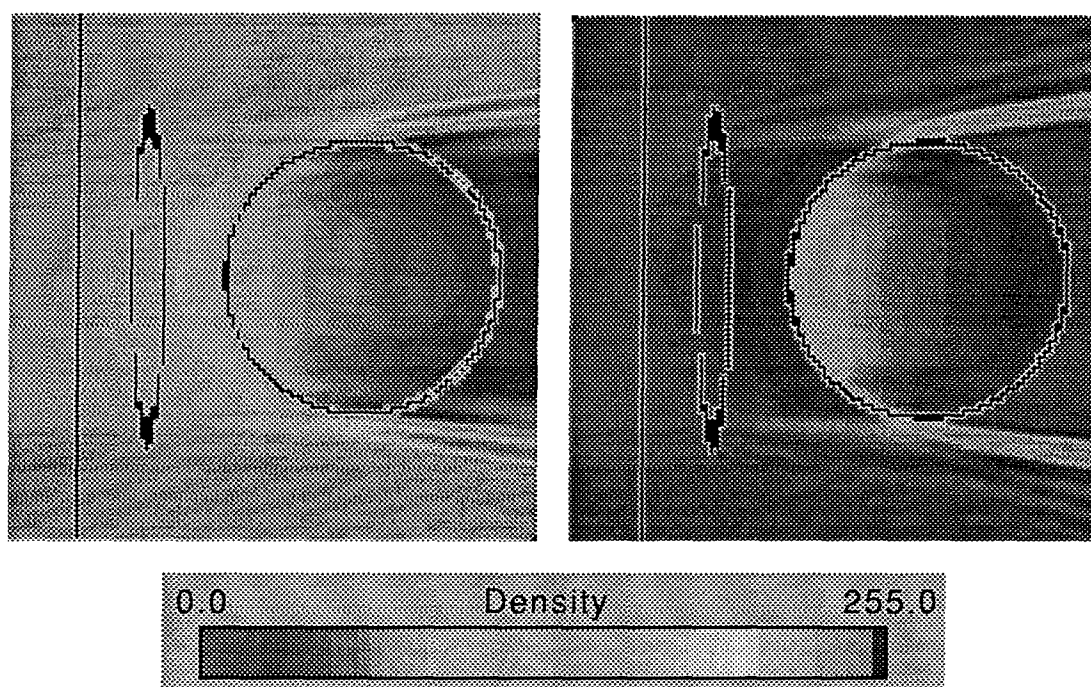


Figure 5: Shown on the left is the predicted wave energy density produced by an incident continuous plane wave. On the right is shown the density of the energy absorbed by the tissue.

Model Accuracy

While the finite element model is apparently quite accurate it is necessary to establish conditions on boundaries of the modeled region. Since these boundaries are artificially set in the model, the conditions at the boundary must be for free space radiation. These conditions, as established in our model, were not sufficiently accurate, and there were standing waves set up in the computational grid that were spurious. Changing model geometry and boundary conditions would affect, but not eliminate these spurious waves. This problem with the boundary conditions, along with the speed issues discussed above have resulted in the rejection of the FE model as an option for our current research.

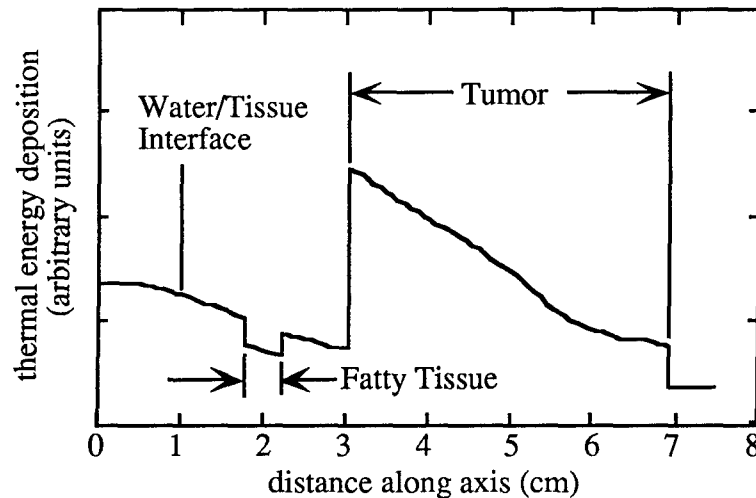


Figure 6: Thermal energy deposition along a central axis predicted by the parabolic model.

The verification of the parabolic marching method is discussed below. The "gold standard" in the initial tests has been analytic spherical Bessel function solutions for simple geometries that have analytic solutions. For the complicated cases encountered in the laboratory, we will use the integral equation solutions.

The following figures demonstrate the agreement between the integral equation method and the parabolic method. Figure 7 shows the geometry used for this analysis. Figure 8 shows a color mapped representation of a slice of the field. Figure 9a and 9b show the results using a speed of sound in the sphere significantly less than and significantly greater than that of water. Given the differences in the two models, one would expect error to increase as the mismatch in sound velocity between the tumor and water increases. Thus, these two conditions should represent worst case errors. Figure 10 is an axial plot of the same data.

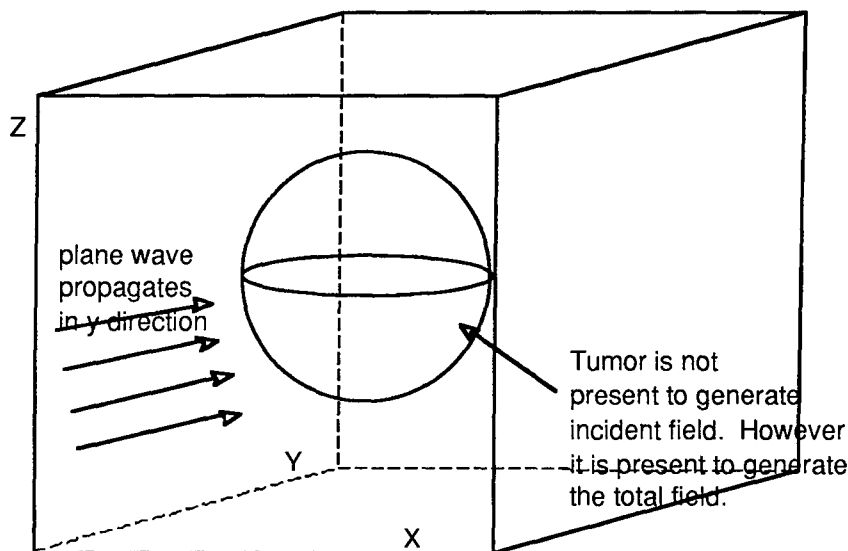


Figure 7: Model geometry for accuracy comparisons.

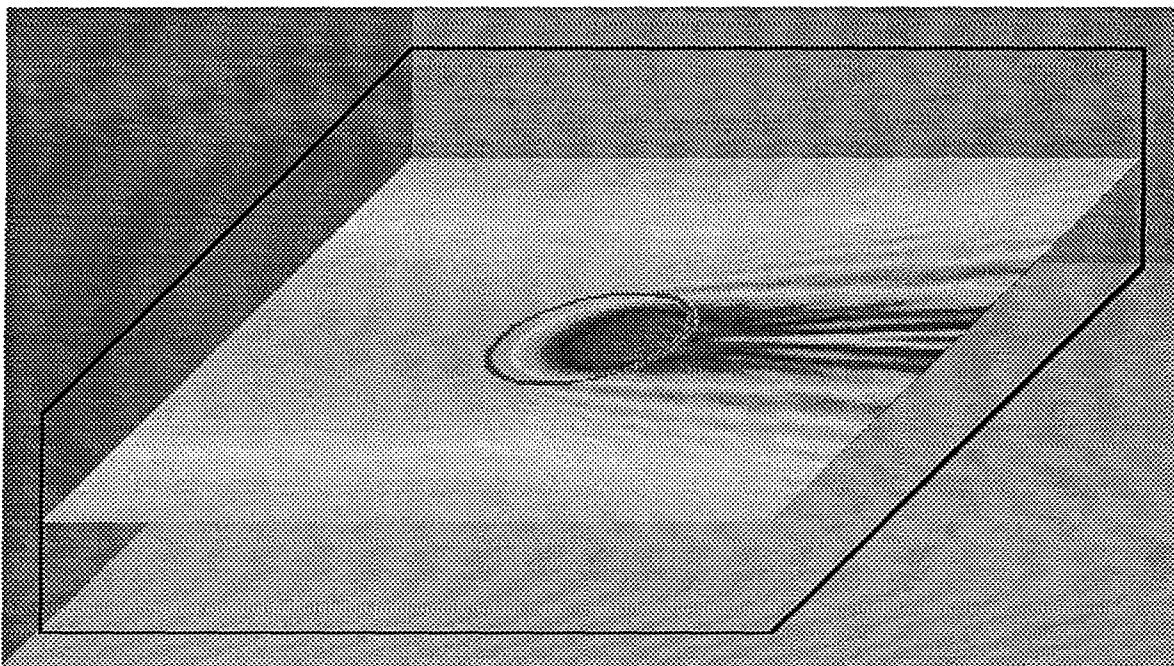


Figure 8: This is a color mapped image of the power deposition in the model shown in Figure 7.

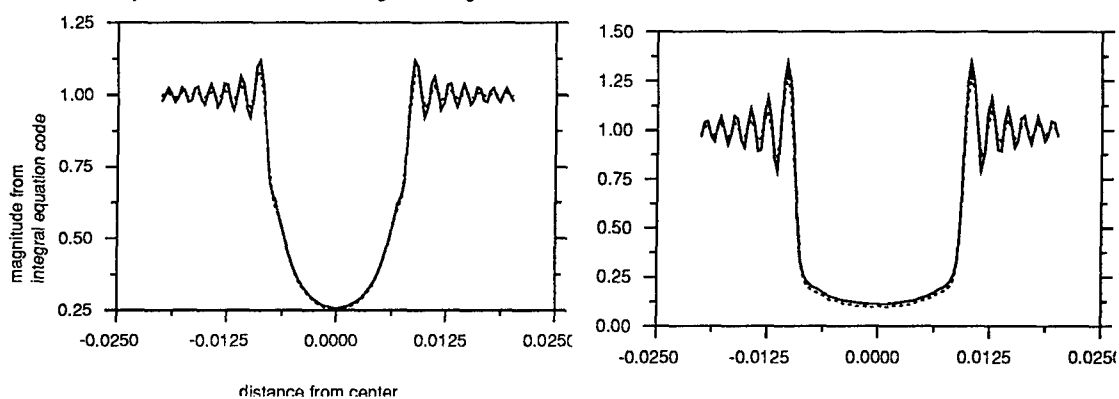


Figure 9: a) The speed of sound internal to the sphere was 1267.7 m/sec, substantially less than that which would be encountered in the breast, thereby making the impedance contrast quite a bit larger than is likely to be encountered in practice. b) Here the speed of sound internal to the sphere was 1677 m/sec, which is substantially greater than any tumor that would be found in the breast. Here the solid line represents the integral model and the dashed line represents the parabolic model.

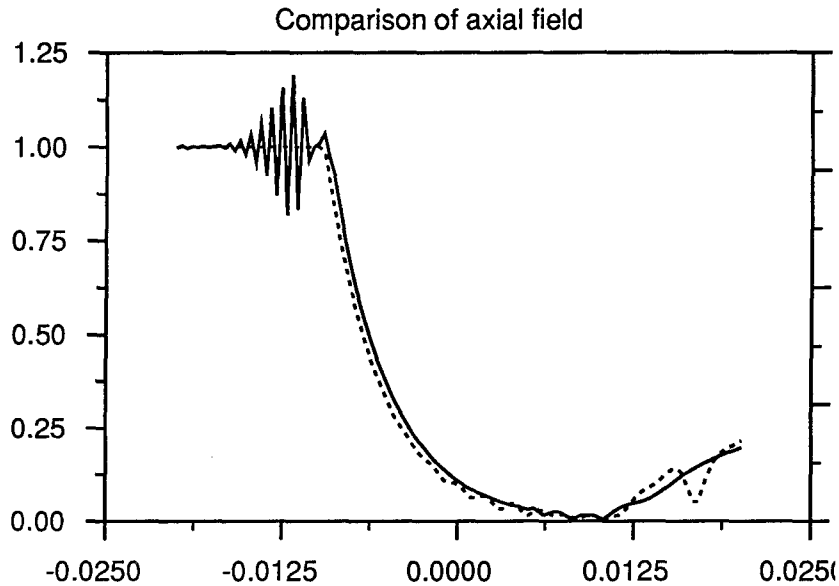


Figure 10: The integral equation is shown in solid, and shows the diffraction pattern due to reflections from the hard sphere. This plot shows quantitatively that the parabolic method does not take into account the reflections of sound waves. Conditions for this graph correspond to those in Fig. 9b.

The excellent match between the two models in the forward scattered diffraction patterns shown in Fig. 9 and the poor match in the reflected diffraction pattern shown in Fig. 10 highlights the differences between the two models. The excellent overall match between the two models in this worst case condition, coupled with the enormous speed enhancement associated with the parabolic model makes it an excellent candidate for our application.

Subsystem 4: Inverse Optimization Technique

Inverse Techniques

Inverse problems arise when the physical environment either severely limits or completely prohibits the direct measurement of the parameters necessary to uniquely determine a system's dependent variables. When using ultrasound hyperthermia to treat breast cancer the parameters of interest are the spatial distribution and values of: (a) tissue density, (b) acoustic pressure amplitude attenuation coefficient and (c) wave speed. The wave speed and acoustic pressure amplitude attenuation coefficient can be treated as one quantity in terms of the complex wave number. The dependent variable of interest is the absorbed power, (q).

If one knows all the parameters of a problem then it is possible to solve the "forward" problem for the dependent variables using the differential wave equation. The inverse problem arises when one does not know the parameters but is able to measure some other property of the system, usually some of the dependent variables. For ultrasound hyperthermia of breast cancer it is possible to pre-determine geometric regions of constant property (see Subsystem 1) and then measure on-line the value of the absorbed power (see Subsystem 2) at a limited number of internal points --- the thermocouple junctions.

The inverse technique developed for this research utilizes a standard inverse technique for non-linear problems[20] that is based on minimizing the error between the model estimated absorbed powers and the clinically measured absorbed powers. The minimization is accomplished by changing the value of the unknown parameters in the model until the "cost" function,

$$\Phi(e) = \sum_{i=1}^{Nm} e_i^2 \quad \text{Equation [1]}$$

where

$$e_i = \langle q_v \rangle_i^{\text{measured}} - \langle q_v \rangle_i^{\text{modeled}}$$

is minimized. This technique is also termed *parameter estimation*. The inverse process begins by assuming some value for the unknown parameters and solving the "forward" problem. The error between the model estimated dependent variables and the measured dependent variables and the resulting changes in absorbed power are given by the following linear approximation:

$$[J] (\Delta\gamma) = (e) \quad \text{Equation [2]}$$

The "Jacobian" matrix, **J**, is constructed from numerical simulations and is given by

$$\mathbf{J} = \begin{bmatrix} \frac{\partial \langle q_v \rangle_1}{\partial \gamma_1} & \frac{\partial \langle q_v \rangle_1}{\partial \gamma_2} & \dots & \frac{\partial \langle q_v \rangle_1}{\partial \gamma_{Np}} \\ \frac{\partial \langle q_v \rangle_2}{\partial \gamma_1} & \frac{\partial \langle q_v \rangle_2}{\partial \gamma_2} & \dots & \frac{\partial \langle q_v \rangle_2}{\partial \gamma_{Np}} \\ \vdots & \vdots & \ddots & \vdots \\ \frac{\partial \langle q_v \rangle_{Nm}}{\partial \gamma_1} & \frac{\partial \langle q_v \rangle_{Nm}}{\partial \gamma_2} & \dots & \frac{\partial \langle q_v \rangle_{Nm}}{\partial \gamma_{Np}} \end{bmatrix} \quad \text{Equation [3]}$$

The inverse method utilized herein follows the following cycle of calculations in which the model parameters, γ , are updated according to equation [2] until there are negligible changes.

1. Using the current values of model parameters, γ , calculate the Jacobian in equation [3]
2. Construct the error vector using the current values of model parameters, γ
3. Invert equation [2] using singular value decomposition (SVD) to solve for changes in model parameters, γ
4. Update model parameters
5. Stop if the change in model parameters is small or the error, e , is acceptable

Future Work

Third year efforts will involve parallel efforts in all four subsystems:

- Subsystem 1: A hardware system will be developed to allow the geometry acquisition to be automated. Software development will continue, moving toward defined clinical methods for geometry acquisition and attenuation estimation.
- Subsystem 2: Software for the experimental plan discussed above will be implemented. Clinical tests for this subsystem are anticipated.
- Subsystem 3: A final model will be selected and work will begin to produce an automatic interface between Subsystem 3 (the model) and the other subsystems.
- Subsystem 4: Software development will continue. Beginning with simulated data, then using clinical data when it is available from Subsystem 2, the algorithm will be debugged and tested.

References

- [1] Anonymous., *JAMA*, 271:797-802, 1994.
- [2] B.A. Bornstein, P.S. Zouranian, J.L. Hansen, S.M. Fraser, L.A. Gelwan, B.A. Teicher, and G.K. Svensson, *Int. J. Radiation Oncology Biology Physics*, 25:79-85, 1993.
- [3] J. Overgaard, D.G. Gonzalez, M.C.C.M. Hulshof, G. Arcangeli, O. Dahl, O. Mella, and S.M. Bentzen, *Lancet*, 345:540-543, 1995.
- [4] M. Jolley, Masters Thesis, University of Utah, 1996.
- [5] D.M. Sullivan, R. Ben-Yosef, and D.S. Kapp, *Int. J. of Hyperthermia*, 9(5):627-643, 1993.
- [6] The program FASTQ was obtained in the ACCESS package from Sandia National Laboratories, Albuquerque, New Mexico 857185-0441, attn: Organization 1503
- [7] G. Berger, P. Laugier, J.C. Thalabard, and J. Perrin, *Ultrasonic imaging*, 12:47-57, 1990.
- [8] B.W. Dong, M. Wnag, K. Xie, and M.H. Chen, *J. Clinical Ultrasound*, 22:167-174, 1994.
- [9] S.W. Flax, J.P. Norbert, G.H. Glover, F.D. Gutmann, and M. McLachlan, *Ultrasonic Imaging*, 5:95-116, 1983.
- [10] B.S. Garra, M.F. Insana, T.H. Shawker, and M.A. Russell, *Radiology*, 162:61-67, 1987.
- [11] M. Fink, F. Hottier, and J.F. Cardoso, *Ultrasonic Imaging*, 5:117-135, 1983.
- [12] S.A. Goss, R.L. Johnson, F. Dunn, *JASA*, 64:423-457, 1978.
- [13] W.J. Fry and R.B. Fry, *JASA*, 26(3):311-317, 1954.
- [14] W.J. Fry and R.B. Fry, *JASA*, 26(3):294-310, 1954.
- [15] C.J. Martin and A.N.R. law, *Ultrasonics*, 18:127-133, 1980.

- [16] C.J. Martin, K. Hynynen, and D.J. Watmough, *Ultrasound in Medicine and Biology*, 10(6):701-708, 1984.
- [17] K.J. Parker, *JASA*, 74(5):1356-1361, 1983.
- [18] A.A.C. De Leeuw, J. Crezee, and J.J.W. Lagendijk, *Int. J. of Hyperthermia*, 9(5):685-697, 1993.
- [19] W.L. Nyborg, *JASA*, 70(2):310-312, 1981.
- [20] Y. Bard, *Nonlinear Parameter Estimation*, Academic Press, Inc., New York, 1974.
- [21] M. Lyons and K.J. Parker, *IEEE Trans Ultrason Ferroelectr Freq Control*, 35:511-521, 1988.
- [22] R. Kuc and M. Schwartz, *IEEE Transactions on sonics and Ultrasonics*, SU-26:353-362, 1979.
- [23] R. Kuc and K. J. W. Taylor, *Ultrasound in Medicine and Biology*, 8(4):403-412, 1982.
- [24] M. D. Collins, *JASA*, 91:1357-1368, 1992.
- [25] F. Natterer and F. Wübbeling, *Lecture Notes in Physics*, 422:157-166, 1993.
- [26] R. H. Hardin and F. D. Tappert *SIAM Rev.* 15:423, 1973.
- [27] M. D. Collins, *JASA*, 93:1736-1742, 1993.
- [28] M. E. Taylor, *Pseudo-differential Operators*, Princeton University Press, Princeton, 1981.
- [29] D.W. Pepper and J.C. Heinrich, *The Finite Element method: Concepts and Applications*, Hemisphere Publishing Corporation, Washington, 1st Ed., 1992.
- [30] H. Gan, P.L. Levin, and R. Ludwig, *JASA*, 94(3):1651-1662, 1993.

Appendix A: LOG SPECTRAL DIFFERENCE

The log spectral difference method is a technique of determining an ultrasound pressure amplitude attenuation coefficient (UPAAC), based on the power spectrum of a reflected ultrasound signal.[8,9,11] The idea behind this technique is to compute the normalized attenuation coefficient, β , by determining the reduction in amplitude of the spectrum. The UPAAC, α , is then calculated from Equation A1, where β is the attenuation coefficient normalized to both frequency and depth, and f is the frequency. Depending on the type of tissue, n has been found to be between 1 and 1.3.[21]

$$\alpha = \beta f^n \quad \text{Equation [A1]}$$

To simplify the calculations, a linear relationship between α and f ($n=1$) is assumed. The process of calculating β will be discussed in the following paragraphs.

Determining β begins with analyzing the reflected radio frequency (RF) signal of a pulse sent from an ultrasound transducer into the tissue of concern. Portions of the signal originating from the front and back areas of the region of interest are chosen. The shallow region is selected to be the tissue segment just after a tissue interface, because the irregular geometry and surface roughness at the interface will scatter the ultrasound wave and produce inaccurate results. The deep region is chosen before a tissue interface for the same reason. The optimal distance between the two chosen regions has been shown by Kuc to be two-thirds of the region of interest (see Figure A1).[22,23] A typical RF signal received from a pulse sent into tissue is shown in Figure A2. The portions of the signal associated with the shallow and deep regions are marked on the figure. However, these segments of the signal are not isolated.

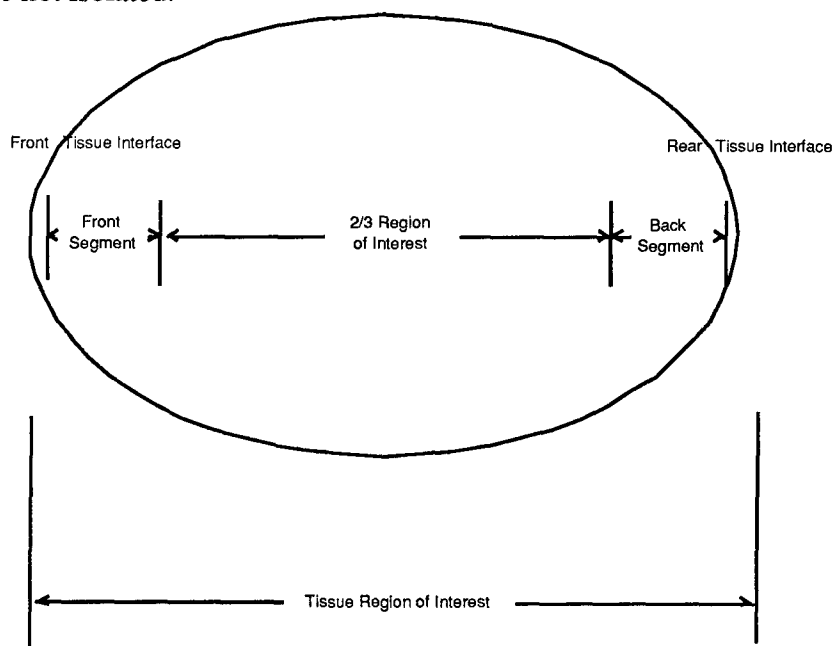


Figure A1: The ellipse represents a tissue region of interest (tumor, organ, etc.).

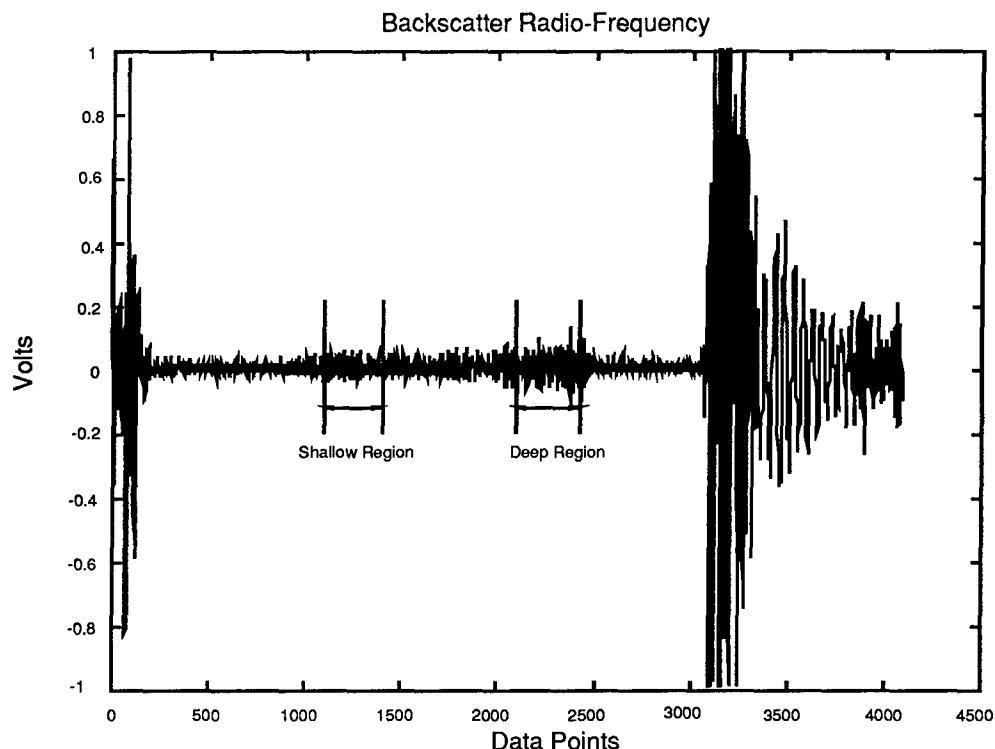


Figure A2: This represents the RF waveform of a single A-line collected from the B-scan imager. Two regions selected from the object in Fig. A1 are indicated.

The regions selected from the RF signal contain overlapping reflections from different areas of tissue. To reduce the many complexities associated with this phenomenon, the signal from each region is divided into overlapping sections, and each section is windowed using a Hanning or similar window. Next, the log of the Discrete Fourier Transform (DFT) is calculated for each section to form the power spectrum. This spectrum, exhibited in Figure A3, is for the shallow and deep segments of Figure A2.

In the power spectrum form, the signal can be quickly analyzed. The power spectrum of the deep region is subtracted from the spectrum of the shallow region, leaving a single line representing the log spectral difference (thus the name of the method). The slope of this line, ω , is calculated using linear regression. Figure A4 shows the result after the power spectrum of the deep and shallow segments have been subtracted and linear regression has been performed. After the slope of the line is found, it is divided by the round-trip distance between the chosen segments giving the normalized attenuation coefficient, β , as shown in Equation A2.

$$\beta = \frac{\omega}{2(x_2 - x_1)} \quad \text{Equation [A2]}$$

The variables x_1 and x_2 represent the distances to the shallow and deep segments respectively. After β is determined, the UPAAC can be calculated as demonstrated previously.

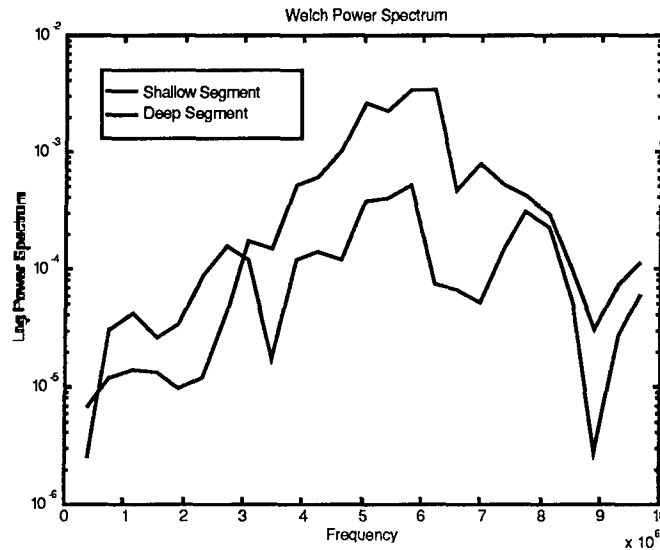


Figure A3: The log of the magnitude of the RF waveform for the deep and shallow regions is plotted as a function of frequency.

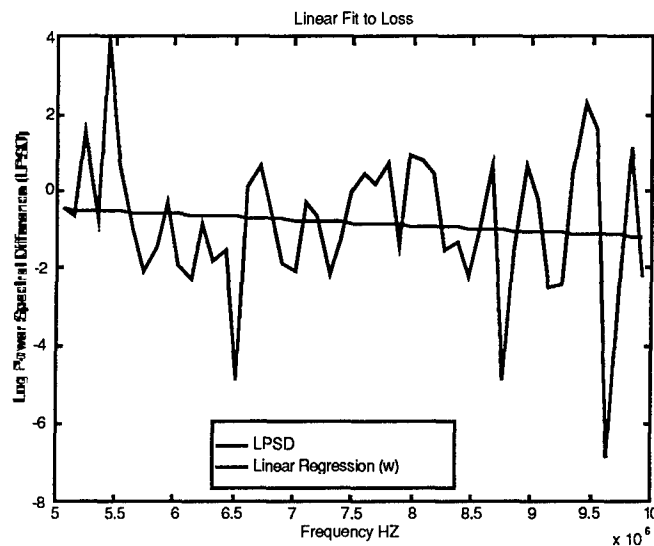


Figure A4: By subtracting the two curves from Figure A3, the Log Spectral Difference is formed.

The UPAAC calculated from a single RF signal is not a reliable measurement of acoustic attenuation. Discontinuities and other distortions in the tissue will skew the results if only one RF signal is analyzed to determine α . To avoid any anomalies that may be present in a single signal, the results from the analyses of several contiguous signals should be averaged together. This will produce a more accurate and precise method of determining the UPAAC value for a given substance.

Appendix B: ULTRASOUND PROPAGATION MODELS

Parabolic Equation Fourier Marching Method

Introduction

The parabolic equation method is a very efficient method for modeling acoustic wave propagation through low contrast acoustic materials (such as breast tissue). The original or classical method requires for its applicability that energy propagate within approximately $\pm 20^\circ$ from the incident field direction. Later versions allowed propagation at angles up to $\pm 90^\circ$ from the incident field direction. Further modifications provide accurate backscattering information, and thus are applicable to the higher contrasts encountered in nondestructive imaging, EM and seismic applications.[24,25]

The source/receiver geometry used in the hyperthermia experiment, and the relatively low contrast of breast tissue, allow us to utilize this efficient approximation. The resulting speed-up relative to the finite element method is dependent upon the contrast but is found to be fairly large. This is especially true of the large 3D problems simulated in this report. We have found that there is difficulty in using standard mesh-generating code to model a 7.5 by 7.5 by 7.5 cm piece of tissue at 500 KHz. However, we have carried out simulations at the full 2 MHz using the Parabolic Fourier Marching method. The operating frequency of the device is 2 MHz so we are confident that the present code will serve as a suitable model, provided, of course that the accuracy can be verified. The verification of the parabolic marching method has been successfully carried out for smaller problems, but is still to be tested for the larger 3D problems that are required for this report. The "gold standard" in the initial tests has been analytic spherical Bessel function solutions for simple geometries that have analytic solutions. For the complicated cases encountered in the laboratory, we will use the integral equation solutions. Furthermore the coarse grain parallelization employed in the integral equation method is equally applicable to the parabolic algorithm.

The Parabolic equation approximation, and more exactly, the "split step Fourier Method" is a new method based upon earlier literature.[26,27]

The source/receiver geometry requirements and the relatively low contrast of breast tissue, allow us to utilize this efficient approximation, for breast cancer scanner and hypothermia applications, for example. In particular because we may elect to use only transmission data in the breast hyperthermia problem, we are able to use this "parabolic approximation" in a straight-forward, simple manner [26]. The Parabolic method can be adjusted, however, to include the effects of backscatter, although this approximation increases the computational complexity of the algorithm.

Discussion and Derivation of Fourier marching method

To derive and elucidate the parabolic equation method, we begin with the 2-D Helmholtz wave equation governing wave propagation in inhomogeneous media:

$$\left\{ \frac{\partial^2}{\partial x^2} + \left(k^2(x, y) + \frac{\partial^2}{\partial y^2} \right) \right\} f(x, y) = 0$$

Equation [B1]

Now Fourier transforming y to λ results in:

$$\left[\frac{\partial^2}{\partial x^2} + \left(\frac{1}{2\pi} \hat{k}^2(\lambda) * -\lambda^2 \right) \right] \tilde{f}(x, \lambda) = 0 \quad \text{Equation [B2]}$$

where:

$$\hat{k}^2(\lambda) \equiv \hat{k}^2(x, \lambda) \equiv \int_{-\infty}^{\infty} k^2(x, y) e^{-i\lambda y} dy \quad \text{Equation [B3]}$$

and the $*$ notation denotes convolution:

$$f(\lambda) * g(\lambda) = \int_{-\infty}^{\infty} f(\lambda - \lambda') g(\lambda') d\lambda' \quad \text{Equation [B4]}$$

Eqn. (B2) can be factored in the sense of pseudo-differential operators [28]

$$\left(\frac{\partial}{\partial x} + i \sqrt{\frac{1}{2\pi} \hat{k}^2(\lambda) * -\lambda^2} \right) \left(\frac{\partial}{\partial x} - i \sqrt{\frac{1}{2\pi} \hat{k}^2(\lambda) * -\lambda^2} \right) \tilde{f}(x, \lambda) = 0 \quad \text{Equation [B5]}$$

An intuitive feel for the manner in which the Parabolic equation arises can be seen by looking at particularly simple case: when k is a constant, then we have, upon Fourier Transforming (B1):

$$\left(\frac{\partial}{\partial x} + i \sqrt{k^2 - \lambda^2} \right) \left(\frac{\partial}{\partial x} - i \sqrt{k^2 - \lambda^2} \right) \tilde{f}(x, \lambda) = 0 \quad \text{Equation [B6]}$$

where the square root is now simply the square root of a scalar. From B6, it is clear that in this special case, two solutions exist:

$$\left(\frac{\partial}{\partial x} + i \sqrt{k^2 - \lambda^2} \right) \tilde{f}(x, \lambda) = 0, \quad \tilde{f}(x, \lambda) = g(\lambda) e^{-ix \sqrt{k^2 - \lambda^2}} \quad \text{Equation [B7]}$$

for an arbitrary function g , which represents a right moving wave for $e^{i\omega t}$ time dependence and:

$$\left(\frac{\partial}{\partial x} - i \sqrt{k^2 - \lambda^2} \right) \tilde{f}(x, \lambda) = 0, \quad \tilde{f}(x, \lambda) = g(\lambda) e^{ix \sqrt{k^2 - \lambda^2}} \quad \text{Equation [B8]}$$

representing a wave which "moves" to the left. Suppose that we know that the field is due to sources entirely on the LHS of the x - y plane. Then, for $x > 0$ we must have:

$$\tilde{f}(x, \lambda) = g(\lambda) e^{-ix \sqrt{k^2 - \lambda^2}} \quad \text{Equation [B9]}$$

Note that knowledge of f on the line $x=0$ (boundary condition) completes the solution since:

$$\tilde{f}(0, \lambda) = g(\lambda) \quad \text{Equation [B10]}$$

and so, on inverse Fourier Transforming:

$$f(x, y) = \frac{1}{2\pi} \int_{-\infty}^{\infty} \tilde{f}(0, \lambda) e^{-ix\sqrt{k^2 - \lambda^2}} e^{i\lambda y} d\lambda, \quad x > 0 \quad \text{Equation [B11]}$$

In fact, for any $x_0 > 0$:

$$f(x, y) = \frac{1}{2\pi} \int_{-\infty}^{\infty} \tilde{f}(x_0, \lambda) e^{-i(x-x_0)\sqrt{k^2 - \lambda^2}} e^{i\lambda y} d\lambda, \quad x > x_0 > 0 \quad \text{Equation [B12]}$$

The idea behind the parabolic equation method is to try to factor a general inhomogeneous (i.e. $k=k(x, y)$) problem into forward and backward moving (in x) factors and then solve only the forward (+ x) moving part (assuming that the field source is to the left (on the x -axis) of the scatterer).

Let $x_n = n\Delta$, $n=0, \dots$ then B12 is:

$$f_{n+1}(y) = \frac{1}{2\pi} \int_{-\infty}^{\infty} \tilde{f}_n(\lambda) e^{-i\Delta\sqrt{k^2 - \lambda^2}} e^{i\lambda y} d\lambda \quad \text{Equation [B13]}$$

Since B13 is local to $x=(n+1/2)\Delta$ we consider the discretization/approximation:

$$f_{n+1}(y) = \frac{1}{2\pi} \int_{-\infty}^{\infty} \tilde{f}_n(\lambda) e^{-i\Delta\sqrt{k^2(x_{n+1/2}, y) - \lambda^2}} e^{i\lambda y} d\lambda \quad \text{Equation [B14]}$$

for propagating forward through k that is inhomogeneous in x and y i.e. $k=k(x, y)$, and $f_n(y) = f(x_n, y)$. Computationally (B14) would be an inverse Fourier transform except for the y -dependence of k .

Defining:

$$k_n^2 \equiv k^2(x_{n+1/2})$$

gives:

$$f_{n+1}(y) = \frac{1}{2\pi} \int_{-\infty}^{\infty} \tilde{f}_n(\lambda) e^{-i\Delta\sqrt{k_n^2 - \lambda^2}} e^{i\lambda y} d\lambda$$

Advanced Parabolic Marching Method

Now we desire to take the y -dependence out from under the square root in order that it may then be factored out from under the integral, which will result in the integral being an inverse Fourier Transform, and yield a substantial increase in efficiency. This goal can be achieved *approximately* in the following manner:

$$e^{-i\Delta k_{n,m} \sqrt{1-(\lambda/k_{n,m})^2}} \approx e^{-i\Delta(k_{n,m}-k_n)} e^{-i\Delta k_n \sqrt{1-(\lambda/k_n)^2}}$$

so that, defining $k_{n,m} \equiv k(x_{n+1/2}, y_m)$, and $y_m = m\Delta$, then yields:

$$f_{n+1}(y_m) \approx \frac{1}{2\pi} \int_{-\infty}^{\infty} \tilde{f}_n(\lambda) e^{-i\Delta(k_{n,m}-k_n)} e^{-i\Delta k_n \sqrt{1-(\lambda/k_n)^2}} e^{i\lambda y_m} d\lambda$$

or

$$f_{n+1}(y_m) \approx \frac{e^{-i\Delta(k_{n,m}-k_n)}}{2\pi} \int_{-\infty}^{\infty} \tilde{f}_n(\lambda) e^{-i\Delta k_n \sqrt{1-(\lambda/k_n)^2}} e^{i\lambda y_m} d\lambda$$

Equation [B15]

We have thus approximately maintained the y variation in k , while **simultaneously giving a Fourier Transform** formulation for the field f_{n+1} .

$$f_{n+1}(y) \approx \frac{e^{-i\Delta(k_{n,m}-k_n)}}{2\pi} \int_{-\infty}^{\infty} \tilde{f}_n(\lambda) e^{-i\Delta k_n \sqrt{1-(\lambda/k_n)^2}} e^{i\lambda y} d\lambda$$

and in fact using the notation:

$$\hat{f}(y) \equiv \frac{1}{2\pi} \int_{-\infty}^{\infty} f(\lambda) e^{-i\lambda y} d\lambda$$

to indicate the **Inverse** Fourier Transform, gives:

$$f_{n+1}(y) = \overbrace{\tilde{f}_n(\lambda)}^{\wedge} P_n$$

where P_n is the range dependent propagator defined as:

$$P_n(y) \equiv e^{-i\Delta \sqrt{k^2(x_{n+1/2}) - \lambda^2}}$$

This is one basic equation for the parabolic split step method. Various alternative forms can be used in similar algorithms. A common form for the parabolic equation is derived by using the binomial approximation:

$$\sqrt{1 - \left(\frac{\lambda}{k_n}\right)^2} \approx \frac{1}{2} \left(\frac{\lambda}{k_n}\right)^2$$

in the above integral. This yields a "standard" form of the split-step parabolic equation method:

$$f_{n+1}(y_m) = \frac{e^{-i\Delta k_{n,m}}}{2\pi} \int_{-\infty}^{\infty} \tilde{f}_n(\lambda) e^{i\Delta \frac{\lambda^2}{2k_0}} e^{i\lambda y_m} d\lambda$$

Equation [B16]

Numerical experiments have indicated the superiority of B15 over B16. In Fourier notation, B16 is:

$$f_{n+1}(y_m) = e^{-i\Delta k_{n,m}} F^{-1} \left\{ e^{i\Delta \frac{\lambda^2}{2k_0}} F\{f_n\}(\lambda) \right\}(y_m)$$

Equation [B17]

This is the usual form of the split-step PE method. Our more general equation is (in Fourier notation):

$$f_{n+1}(y_m) = e^{-i\Delta(k_{n,m}-k_n)} F^{-1} \left\{ e^{-i\Delta k_n \sqrt{1-(\lambda/k_n)^2}} F\{f_n\}(\lambda) \right\}(y_m)$$

An interesting interpretation of the split step method is evident from this: The algorithm step consists of an exact propagation a distance of Δ in k_0 (which includes diffraction) followed by a phase shift correction, i.e., multiplication by

$$e^{-i\Delta(k_{n,m}-k_0)}$$

Equation [B18]

which corrects the phase of a plane wave traveling forward.

Numerical Experiments:

The geometry for the first experiment consisted of Figure B1 -- which has cylindrical symmetry about the horizontal axis. The tumor was assumed to be perfectly spherical with a diameter of 4 cm. it was placed on the center axis with the center of the sphere located at a distance of 4 cm from the tissue/water interface. The transducer was assumed to be located on the central axis, with its center located 10 cm from the tissue/water interface. The incident field in the first experiment was assumed to be a plane wave propagating along the y axis. The z axis is the vertical axis, the x-axis is coming out of the page, and the y-axis is the horizontal axis.

Once the pressure field has been calculated via the Fourier Domain Parabolic Propagation method, the equivalent internal thermal energy generation due to ultrasound absorption can be calculated using the formula:

$$Q \equiv \alpha \frac{|P|^2}{Z} \left[\frac{W}{m^3} \right]$$

The formula I use for the complex object function γ is:

$$\gamma(\mathbf{x}) \equiv \left(\frac{k^c(\mathbf{x})}{k_o} \right)^2 - 1 = \left(\frac{k(\mathbf{x}) - i\alpha(\mathbf{x})}{k_o^c} \right)^2 - 1$$

where the complex wavenumber $k^c(\mathbf{x})$ is the spatially dependent wavenumber which includes the attenuation coefficient as its imaginary part. The real part of $k^c(\mathbf{x})$ is the standard wavenumber $\omega/c(\mathbf{x})$, where $c(\mathbf{x})$ is the spatially dependent speed of sound. Therefore the object function γ takes the form:

$$\gamma(\mathbf{x}) = \left(\frac{\omega / c(\mathbf{x}) - i\alpha(\mathbf{x})}{\omega / c_o} \right)^2 - 1$$

or

$$\gamma(\mathbf{x}) = \left(\frac{\omega / c(\mathbf{x}) - i\alpha(\mathbf{x})}{\omega / c_o} \right)^2 - 1 = \left(\frac{c_o}{c(\mathbf{x})} - i\alpha(\mathbf{x}) \frac{c_o}{\omega} \right)^2 - 1$$

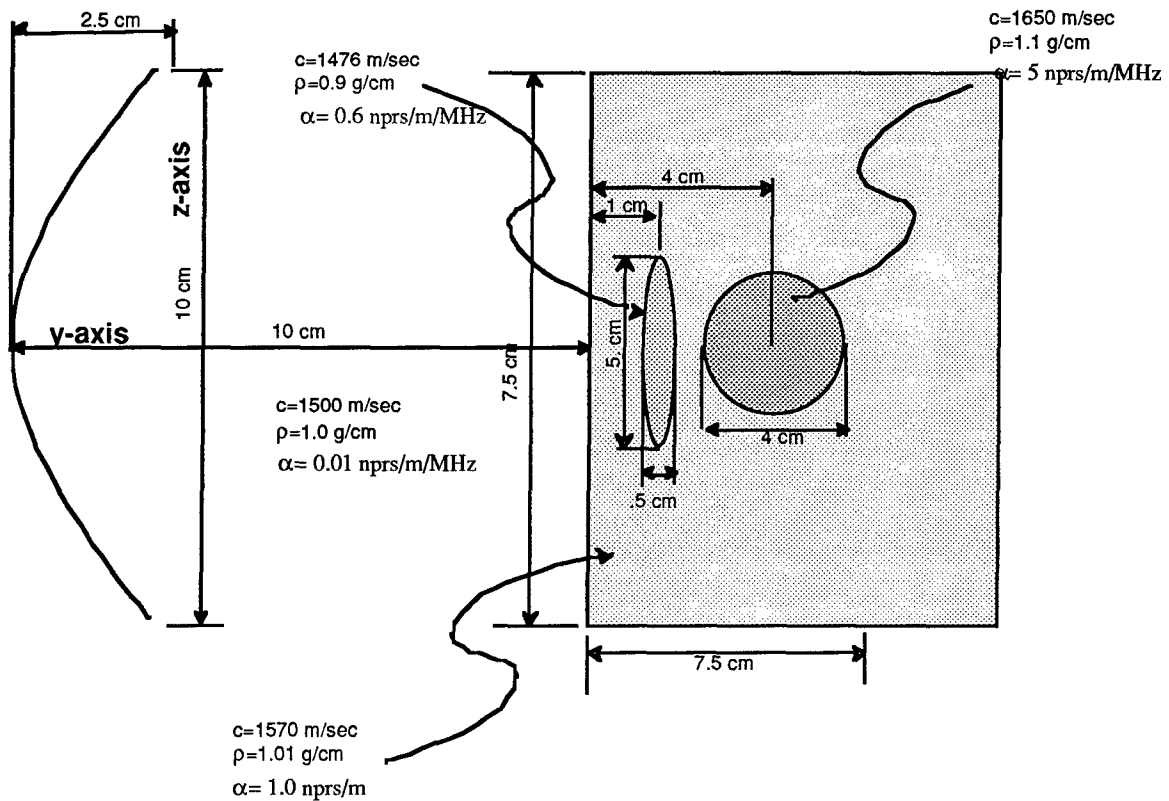


Figure B1: Schematic of the geometry used in the model calculation.

The following table lists the values of the attenuation coefficient in Nepers/m, and real speed of sound in m/sec.

Tissue type	α (Nprs/m)	c (m/sec)
fat	0.6	1476
parenchyma	1.0	1570
tumor	5	1650
water	0.01	1500

Plane Wave Incident Field Simulation:

The following pictures show the results from the simulation of a plane wave impinging upon the tissue/water interface (the first vertical line encountered moving from left to right), the fatty ellipse, (shown in outline in this cross-section), and the spherical tumor (shown in cross section as a circle). The color map is shown below the cross-section, the z axis is vertical, the x-axis comes out of the page, and the y-axis goes left to right in the plane of the paper.

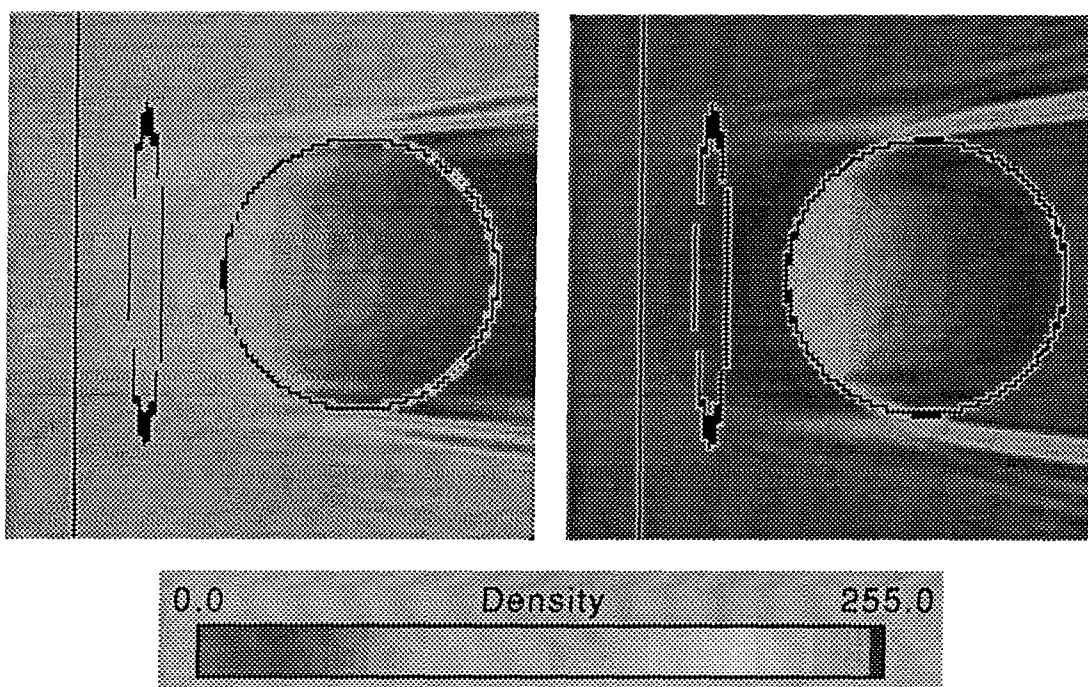


Figure B2: Shown on the left is the predicted wave energy density produced by an incident continuous plane wave. On the right is shown the density of the energy absorbed by the tissue.

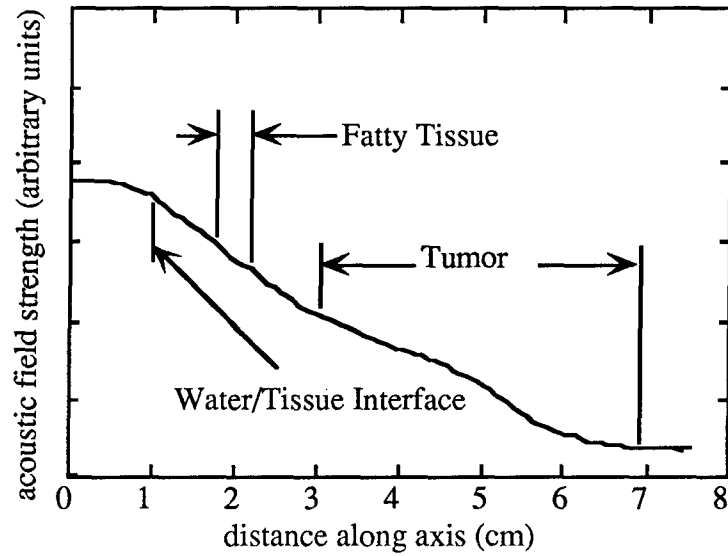


Figure B3: Acoustic field strength along a central axis.

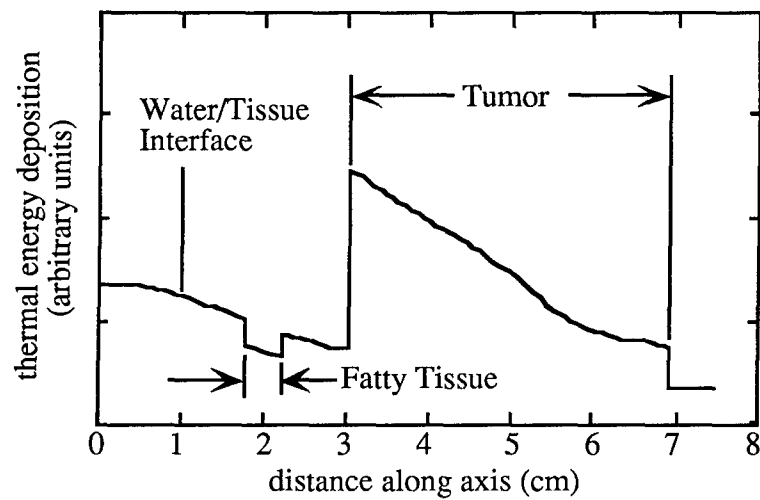


Figure B4: Thermal energy deposition along a central axis.

Focused Incident Field

Now we look at thermal energy deposition in the case of an incident field which is focused at the center of the spherical tumor.

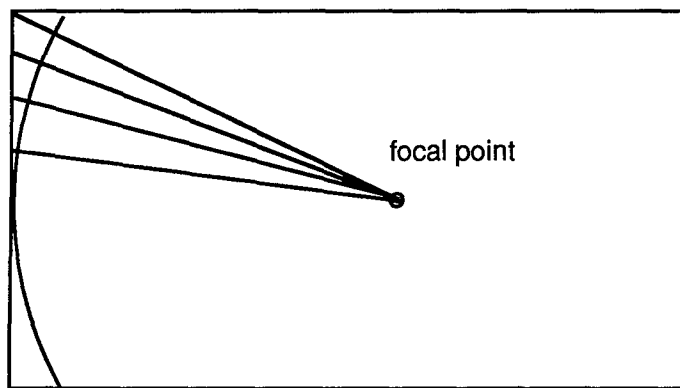


Figure B5: This is a schematic of the focused transducer used in the model.

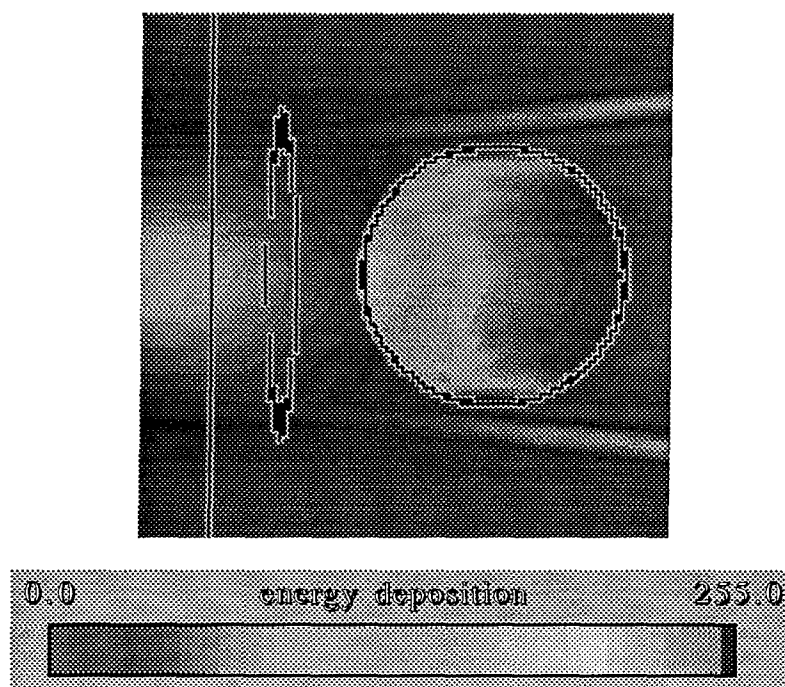


Figure B6: Energy deposition for focused beam

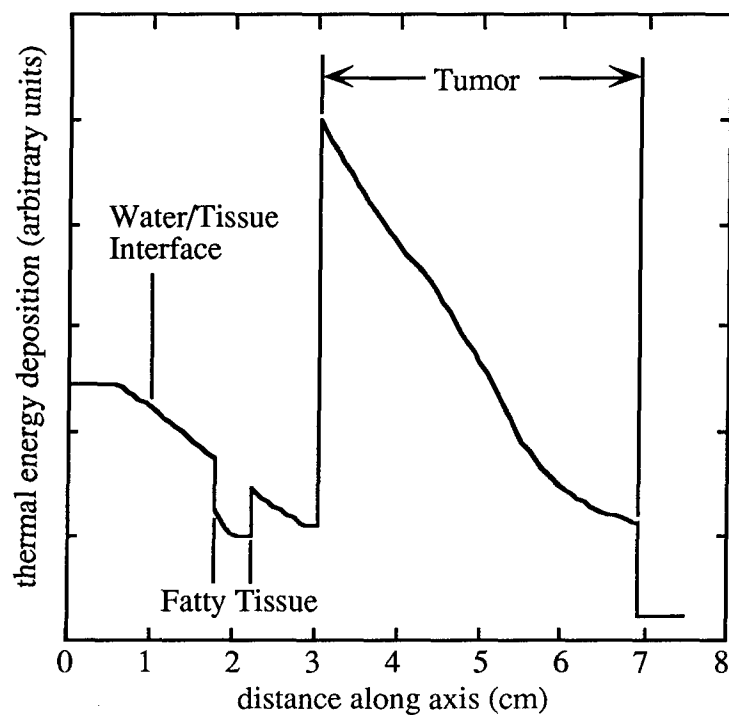


Figure B7: Thermal energy deposition along a central axis.

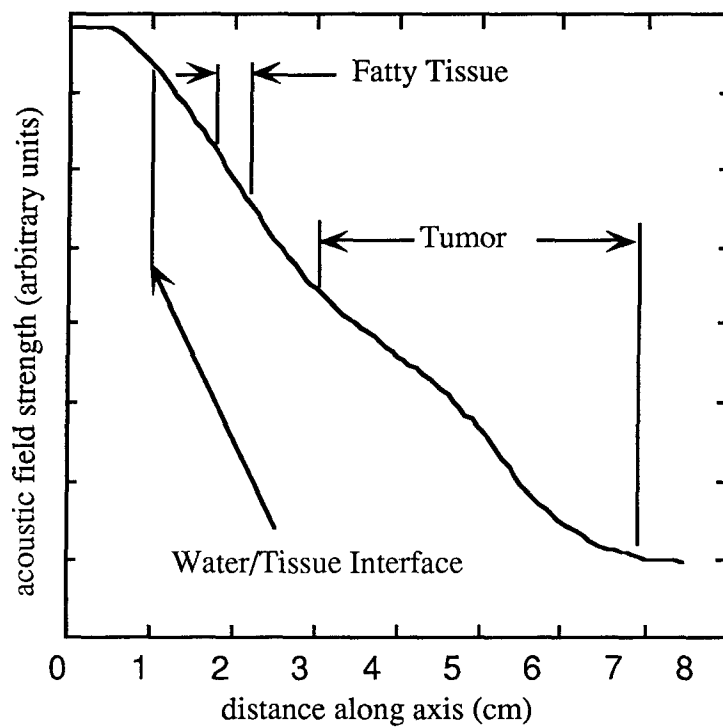


Figure B8: Acoustic field strength along a central axis.

Hybrid Numerical Method

The hybrid numerical method is a combination approach to solving for the pressures arising from the wave equation for the propagation of sound waves through heterogeneous materials. The method uses the Kirchhoff Diffraction Integral to calculate the pressures in the homogeneous water bath region and the Finite Element Method (FEM) for the inhomogeneous tissue region (see Figure B9).

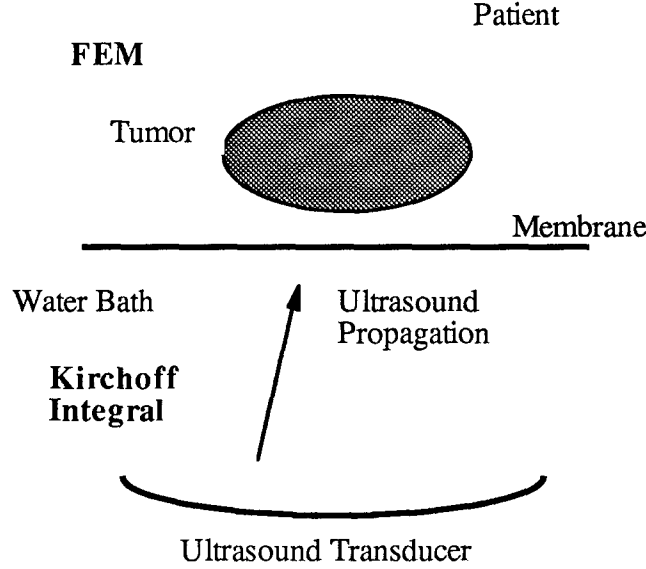


Figure B9: Diagram of the clinical situation for a hyperthermia treatment of the breast or chest wall area.

The ultrasound wave equation for the complex pressures is given by the following equation:

$$\nabla \cdot \left(\frac{1}{\rho^*(\mathbf{x})} \nabla \tilde{p}(\mathbf{x}) \right) + \frac{\tilde{k}^2(\mathbf{x})}{\rho^*(\mathbf{x})} \tilde{p}(\mathbf{x}) = 0, \quad \text{Equation [B19]}$$

the pressure, \tilde{p} and wave number, \tilde{k} are complex quantities. To solve this equation, a hybrid method is used which takes advantage of different numerical methods that are more appropriate for different parts of the domain.

Kirchoff Diffraction Integral:

For the homogeneous water bath, the Kirchhoff Diffraction Integral (B20) is used to

$$\tilde{p}(\mathbf{x}) = -\frac{1}{4\pi} \int_{S_1} \frac{e^{i\tilde{k}R}}{R} \mathbf{n}' \cdot \left[\nabla \tilde{p} + i\tilde{k} \left(1 + \frac{i}{\tilde{k}R} \right) \frac{\mathbf{R}}{R} \tilde{p} \right] da' \quad \text{Equation [B20]}$$

solve for the pressures arising from the ultrasound transducer. The primary purpose of this integral solution is to generate boundary conditions at the water bath - membrane interface that are used by the Finite Element Method described below. The following assumptions are made in this formulation: no reflections and no refractions at the water bath - membrane interface. This method is fast and changes in the tissue regions do not impact the solution of (B20). Consequently, only a smaller region of the overall domain needs to be considered when material properties and tumor locations vary.

Finite Element Method (FEM)

The solution of the acoustic wave equation (B19) can be achieved by directly solving the governing partial differential equation through application of appropriate numerical techniques such as the finite element method. There are typically two stages of this method, the preprocessing stage and the solution phase. The preprocessing stage is accomplished using an unstructured mesh generator, FASTQ, to generate a set of non-overlapping quadrilateral elements. The solution phase can be developed utilizing any standard finite element method since the wave equation is self-adjoint [29,30]. In this case, application of the methods of weighted residuals results in the following identity,

$$\int_{\Omega} W \left[\nabla \cdot \left(\frac{1}{\rho^*(\mathbf{x})} \nabla \tilde{p}(\mathbf{x}) \right) + \frac{\tilde{k}^2(\mathbf{x})}{\rho^*(\mathbf{x})} \tilde{p}(\mathbf{x}) \right] d\Omega = 0. \quad \text{Equation [B21]}$$

Integrating by parts produces the "weak statement" of the previous identity,

$$\int_{\Omega} W \left[\nabla W \left(\frac{1}{\rho^*(\mathbf{x})} \nabla \tilde{p}(\mathbf{x}) \right) + \frac{\tilde{k}^2(\mathbf{x})}{\rho^*(\mathbf{x})} \tilde{p}(\mathbf{x}) \right] d\Omega = \int_{\Omega} W \frac{1}{\rho} \nabla \tilde{p} d\Omega \quad \text{Equation [B22]}$$

Discretizing \tilde{p} in the usual finite element manner produces the following linear algebraic relation

$$\int_{\Omega} \left[\nabla[W]^T \left(\frac{1}{\rho^*(\mathbf{x})} \nabla[N] \right) + [W]^T \frac{\tilde{k}^2(\mathbf{x})}{\rho^*(\mathbf{x})} [N] \right] d\Omega \{ \tilde{p}(\mathbf{x}) \} = [K] \{ \tilde{p}(\mathbf{x}) \} = 0. \quad \text{Equation [B23]}$$

The complex wave equation does possess one additional complexity not mentioned in the usual finite element texts – the variables are complex numbers.



DEPARTMENT OF THE ARMY

US ARMY MEDICAL RESEARCH AND MATERIEL COMMAND
504 SCOTT STREET
FORT DETRICK, MARYLAND 21702-5012

REPLY TO
ATTENTION OF:

MCMR-RMI-S (70-1y)

22 Jun 00


MEMORANDUM FOR Administrator, Defense Technical Information
Center, ATTN: DTIC-OCA, 8725 John J. Kingman
Road, Fort Belvoir, VA 22060-6218

SUBJECT: Request Change in Distribution Statements

1. The U.S. Army Medical Research and Materiel Command has reexamined the need for the limitation assigned to technical reports written for Award Numbers DAMD17-94-J-4423, DAMD17-94-J-4172, DAMD17-94-J-4367, and DAMD17-94-J-4187. Request the limited distribution statement for Accession Document Numbers **ADB215483**, **ADB234438**, **ADB249605**, **ADB225305**, **ADB232775** and **ADB249636** be changed to "Approved for public release; distribution unlimited." These reports should be released to the National Technical Information Service.

2. Point of contact for this request is Ms. Virginia Miller at DSN 343-7327 or by email at Virginia.Miller@det.amedd.army.mil.

FOR THE COMMANDER:


PHYLIS M. RINEHART
Deputy Chief of Staff for
Information Management